Electronic Supplementary Material (ESI) for Journal of Materials Chemistry C.

Electronic Supplementary Information

Antiphase Boundaries in Truncated Octahedron-shaped Zn-doped Magnetite Nanocrystals

Nerio Fontaiña-Troitiño,[1] Miguel A. Ramos-Docampo,[1] Martín Testa-Anta,[1]
Benito Rodríguez-González,[1] Manuel Bañobre-López,[2] Laura Bocher,[3]
*Keith P. McKenna,[4] Verónica Salgueiriño[1]**

[1]Departamento de Física Aplicada and CACTI, Universidade de Vigo, 36310, Vigo (Spain)

[2]INL – Advanced (magnetic) Theranostic Nanostructures Lab, International Iberian Nanotechnology Laboratory, Av. Mestre José Veiga, Braga (Portugal)

[3]Laboratoire de Physique des Solides, Université Paris-Sud 91405 Orsay (France)

[4]Department of Physics, University of York, Heslington, York YO10 5DD (United Kingdom)

E-mail: vsalgue@uvigo.es

Experimental Section

Zinc-doped magnetite ($Zn_xFe_{3-x}O_4$ (x = 0.25 (sample ***1***), x = 0.50 (sample ***2***), x = 0.8 (sample ***3***), x = 1.0 (sample ***4***))) nanoparticles were obtained by the simultaneous thermal decomposition of zinc and iron precursors (iron (II) acetate (Aldrich, 95%) and zinc (II) acetate dehydrated (Aldrich 98%)) in two different proportions (molar ratio; $Fe(ac)_2/Zn(ac)_2$ = 9.28 (sample ***1***), 5 (sample ***2***), 2.85 (sample ***3***) and 2 (sample ***4***)) to adjust the final stoichiometry. The process was carried out in all the cases using the hot-injection thermal decomposition, that is, injecting both precursors (dissolved in 5 mL of ethanol) in trioctyl amine (TOA) (25 mL, 57.18 mmol) at 180 °C and then left to reflux (at T = 300 °C) for two hours. Once cooled to room temperature, the nanoparticles were separated by centrifugation, washed several times with ethanol and finally dried at room temperature and stored.

Samples for (S)TEM were deposited on a carbon-coated copper grid. TEM images were obtained on a JEOL JEM 1010 microscope operating at 100 kV. (HR)TEM images were acquired on a JEOL JEM 2010F operating at 200 kV. The TEM images were used to obtain the size distribution considering few hundreds of nanoparticles in both samples. STEM-HAADF images were all acquired on the NION UltraSTEM200 operating at 100 kV, yielding a sub-ansgtröm probe size. The XRD patterns of the nanoparticles were obtained with a Phillips PANalytical X'Pert PRO diffractometer using a Cu-K_α radiation in a 2θ range from 20-100°. EDX spectroscopy and ICP analysis were used to determine the stoichiometry of the nanoparticles. Raman spectra were collected with a Renishaw in Via Reflex Raman Microscope. Experiments were conducted at room temperature by using two different excitation wavelengths, that is, λ = 532 nm from a frequency doubled Nd:YAG and Nd:YVO_4 diode laser and λ = 633 nm from a from a He-Ne laser. Magnetic measurements were performed using a Quantum Design (PPMS) magnetometer. Temperature-dependent magnetization curves of the samples were recorded from 5 to 300K at 5 mT under zero-field cooling (ZFC) and field-cooling (FC) conditions. Field-dependent magnetization curves were measured at μ_0H = -5 to 5 T at 5 K and 300 K.

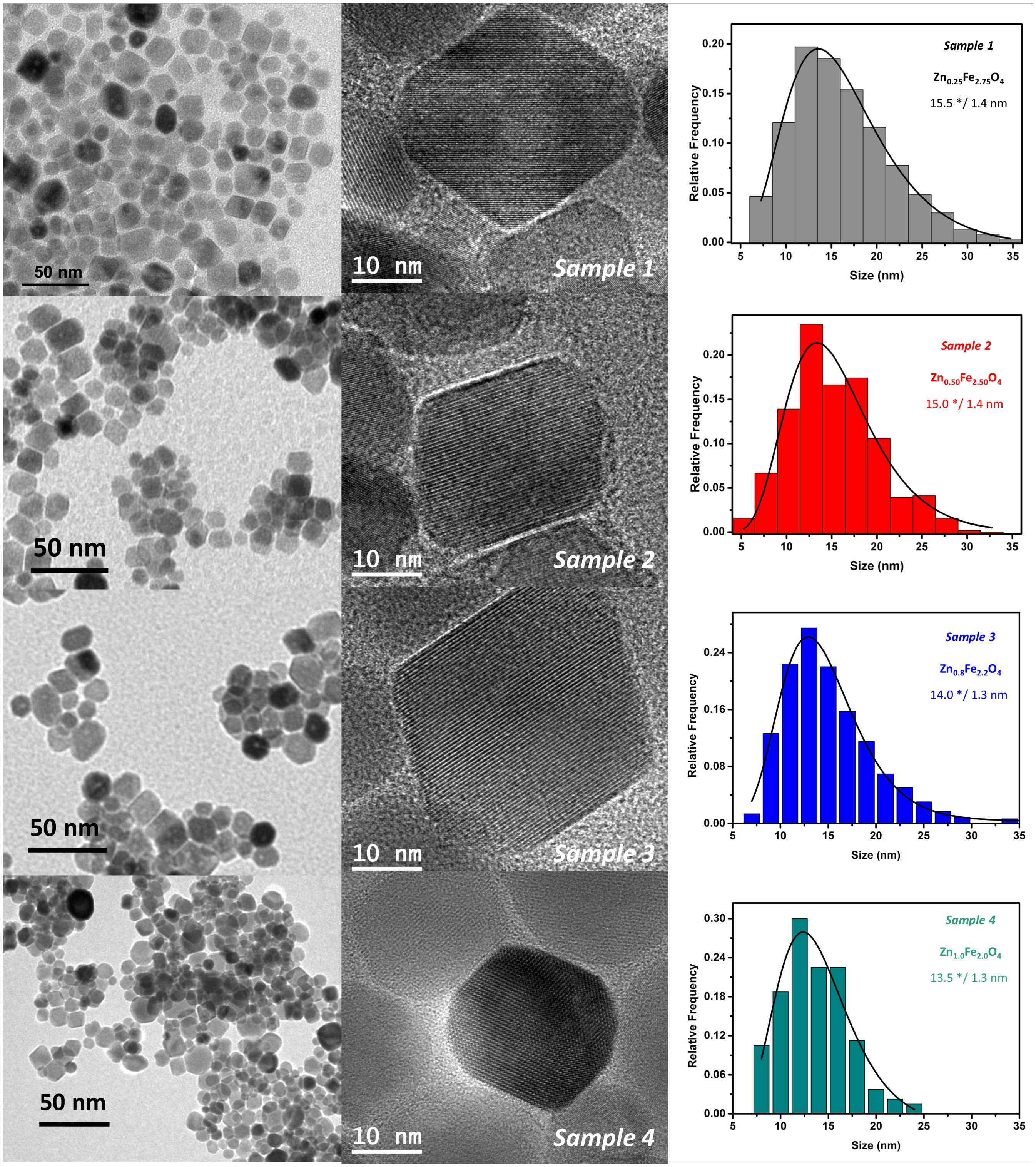

Figure S1. TEM (left column), HRTEM (central column) and size distribution (largest edge length) analysis fitted to lognormal functions (right column), of the zinc-doped magnetite nanocrystals from the four samples in consideration (from top to bottom, sample ***1*** to sample ***4***).

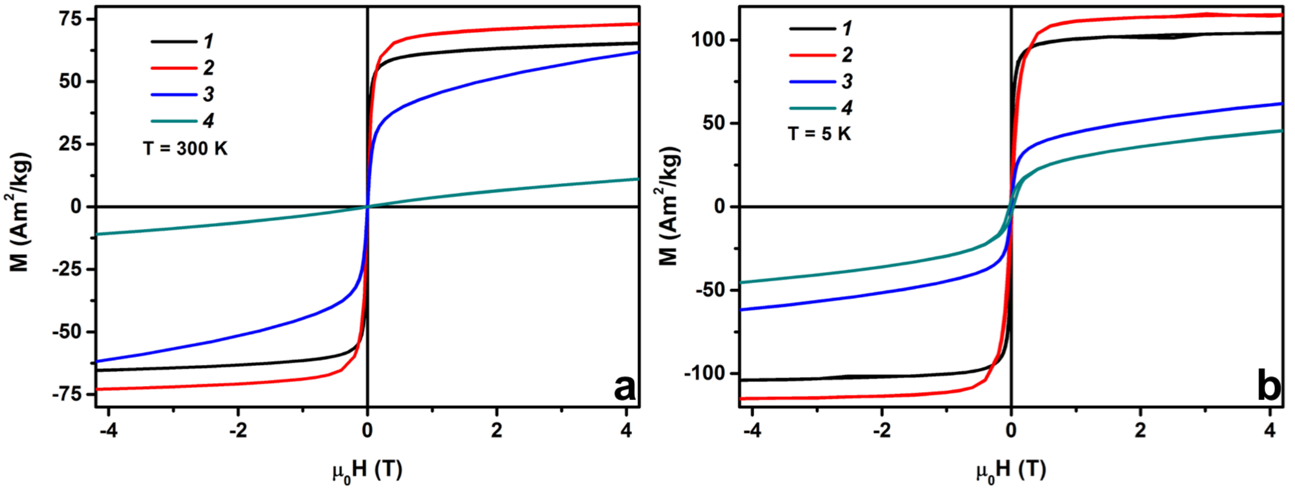

Figure S2. MvsH hysteresis loops at 300 K (a) and 5 K (b) of the zinc-doped magnetite nanocrystals from the four samples in consideration.

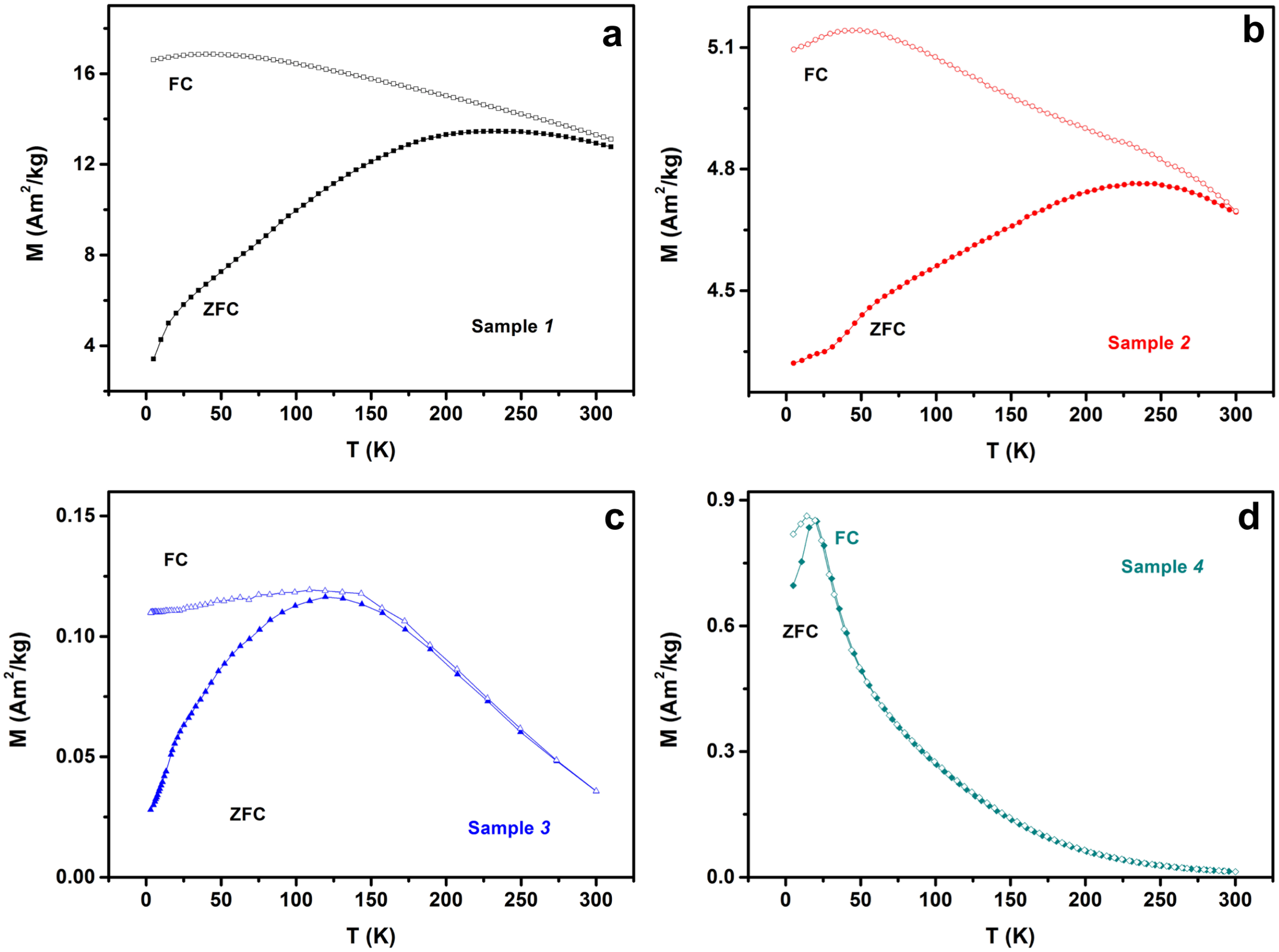

Figure S3. ZFC-FC Temperature-dependent magnetization of the zinc-doped magnetite nanocrystals from the four samples in consideration (sample ***1*** (a), sample ***2*** (b), sample ***3*** (c), and sample ***4*** (d)).

Density functional theory (DFT) calculations

Density functional theory (DFT) calculations to predict the structure, electronic and magnetic properties of bulk $Zn_xFe_{3-x}O_4$ using the projector augmented wave method as implemented in the Vienna *ab initio* simulation package were performed.[1,2] Predictions from several different levels of theory were compared including the Perdew, Burke, and Ernzerhof (PBE) approximation[3,] to exchange and correlation (both with and without Hubbard U corrections on Fe 3*d* states: U-J=3.8 eV – e.g. see reference 4) as well as the Heyd, Scuseria, and Ernzerhof (HSE) hybrid exchange-correlation functional.[5] The 3*s*, 3*d* electrons of Fe, and 2*s* and 2*p* electrons of O were treated as valence electrons and expanded in a plane wave basis with energies up to 400 eV. For primitive cell calculations on the end members Fe_3O_4 (x=0) and $ZnFe_2O_4$ (x=1) a gamma-centred 7x7x7 Monkhorst-Pack (MP) grid was used to sample to Brillouin zone. For the more demanding HSE calculations the MP grid was reduced to 6x6x6 with the Fock exchange potential sampled using a 2 x 2 x 2 grid. To model the compositions present in samples ***1*** and ***2*** ($Zn_2Fe_{22}O_{32}$ (x=0.25) and $Zn_4Fe_{20}O_{32}$ (x=0.50), respectively), a 2x2x1 supercell was employed and all symmetry inequivalent arrangements of Zn within the supercell were considered in order to identify the most stable. For all calculations a number of different orderings of the (collinear) Fe magnetic moments in order to identify the ground state magnetic structure were considered. The total energy was optimized with respect to the position of atoms and the unit cell dimensions using a conjugate gradients algorithm until all forces were less than 0.01 eV $Å^{-1}$. To predict the structure, stability and properties of the (111) antiphase boundary defects (APB) observed in the nanoparticles, a 336-atom supercell containing two domains each about 15 Å in extension perpendicular to the (111) plane was constructed. One domain was rigidly displaced by 3(a/4)(10-1) to create two antiphase boundary (APB) defects in the periodic supercell. The structure of the supercell was optimized with respect to the position of all atoms in the supercell using the methods described above but with a gamma-centred 2 x 2 x 2 MP grid. The total energy was also calculated for similar supercell without the APB displacement (corresponding to a bulk crystal) in order to calculate the APB formation energy.

We first discuss the predicted properties of the two end members of the $Zn_xFe_{3-x}O_4$ series – Fe_3O_4 (x=0) and $ZnFe_2O_4$ (x=1) - at the different levels of theory. The Perdew, Burke, and Ernzerhof (PBE) approximation predicts Fe_3O_4 to be a half-metallic ferrimagnet with lattice constant a = 8.400 Å. The magnetic moment on the tetrahedral Fe (tet-Fe) sites is -3.48 μ_B while the moments on the octahedral Fe (oct-Fe) sites are 3.52 μ_B and 3.61 μ_B. We note the electron density on the oct-Fe sites exhibits a slight disproportionation into two types of site hinting at an intrinsic instability towards a metal-insulator transition, i.e. the Verwey transition. PBE+U also predicts Fe_3O_4 to be a half-metallic ferrimagnet with lattice constant a = 8.470 Å. The magnetic moment on the tet-Fe sites is -4.04 μ_B and between 3.67 and 4.25 μ_B on oct-Fe sites. The Heyd, Scuseria, and Ernzerhof (HSE) calculations performed using the PBE lattice constants predict very similar properties with magnetic moments on the tet-Fe sites of -4.07 μ_B and between 3.90 and 3.95 μ_B on the oct-Fe sites. PBE predicts the $ZnFe_2O_4$ to be an antiferromagnetic insulator with lattice constant a = 8.526 Å. The magnetic moments on the oct-Fe sites are ± 3.66 μ_B and ± 3.76 μ_B (again disproportioning into two types of site). The antiferromagnetic spin configuration is predicted to be 245 meV/formula unit more stable than the ferromagnetic state (i.e. E_{FM}-E_{AF}). PBE+U predicts very similar results with a slightly larger lattice constant of a = 8.512 Å. The magnetic moments on the oct-Fe sites are ± 4.22 μ_B and ± 4.24 μ_B. However, the antiferromagnetic spin configuration is predicted to be only 42 meV / formula unit more stable than the ferromagnetic state. Again, HSE calculations performed using the PBE lattice constants predict very similar properties with magnetic moments on the oct-Fe sites of ± 4.21 μ_B and ± 4.22 μ_B. Overall the above results suggest that both PBE and PBE+U give reasonable predictions for the stable magnetic configuration of $Zn_xFe_{3-x}O_4$ phases with the latter slightly more consistent with the predictions of HSE which is expected to be more accurate (especially for the insulating phases).

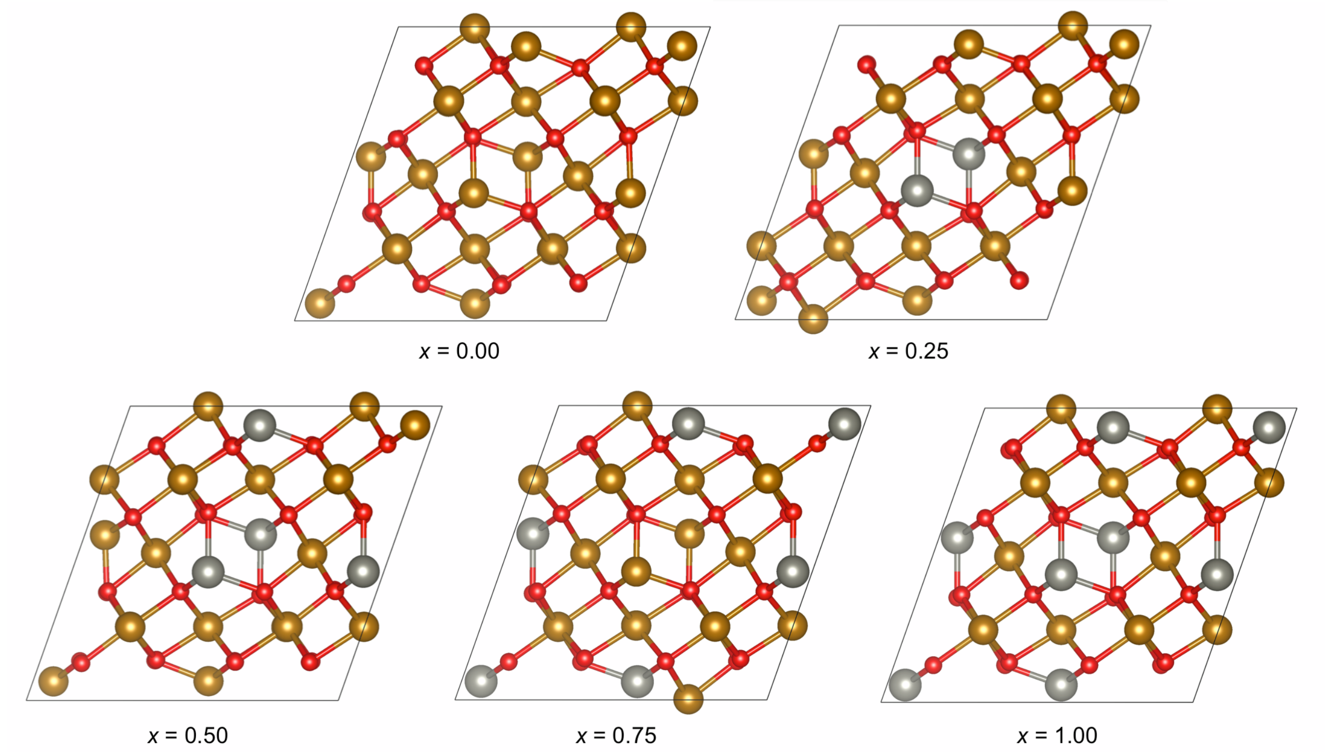

Figure S2. Optimized structures of $Zn_xFe_{3-x}O_4$ at the PBE+*U* level of theory using a 2x2x1 bulk supercell. Silver, brown and red spheres represent Zn, Fe and O atoms respectively.

Table I: Predicted properties of $Zn_xFe_{3-x}O_4$ at the PBE and PBE+*U* levels of theory.

		PBE		
x	**a (Å)**	**Magnetic order**	**Magnetization per formula unit (μB)**	**E_{FM}-E_{AF} per formula unit (meV)**
0.00	8.400	FM	4.00	644
0.25	8.442	FM	5.49	389
0.50	8.484	FM	6.87	178
0.75	8.484	FM	8.11	275
1.00	8.526	AF	0.00	-245
		PBE + U		
x	**a (Å)**	**Magnetic order**	**Magnetization per formula unit (μB)**	**E_{FM}-E_{AF} per formula unit (meV)**
0.00	8.470	FM	4.00	>244
0.25	8.512	FM	5.50	249
0.50	8.512	FM	7.00	121
0.75	8.555	FM	8.50	22
1.00	8.512	AF	0.00	-42

The optimized structures (including optimization of cell volume to within 0.5%) and energies for all symmetry inequivalent arrangements of Zn in a 2x2x1 expansion of the primitive bulk supercell are obtained at both the PBE and PBE+*U* levels of theory. The results are broadly consistent between both levels of theory and figure S2 shows the most stable structures obtained using PBE+*U*. For all compositions there is a preference for Zn to distribute homogeneously throughout the bulk with no evidence of clustering. Zn substitutes for tetrahedral Fe sites and there is a small expansion of the lattice constant associated with increasing Zn content (see Table I). For $x < 1.00$ all structures are predicted to be ferrimagnetic with antiparallel alignment of the moments on the tetrahedral and octahedral Fe sublattices (with the latter being more numerous). As the Zn content increases there is a progressive increase in the total magnetic moment as a result of the reduction in net moment associated with the tetrahedral sites. However, for $x = 1.00$ the antiferromagnetic configuration becomes more stable. We have calculated the energy difference between the ferrimagnetic and antiferromagnetic spin configurations as a function of x at both the PBE and PBE+*U* levels of theory (see E_{FM}-E_{AF} in Table I). A clear crossover between ferrimagnetic and antiferromagnetic order between x=0.75 and x=1.00 is predicted.

References

1. Kresse G.; Furthmüller, J. *Phys. Rev. B* **1996**, *54*, 11169.

2. Kresse G.; Furthmüller, J. *Comput. Mater.Sci.* **1996**, *6*, 15-50.

3. Perdew, J. P.; Burke, K.; Ernzerhof, M. *Phys. Rev. Lett.* **1996**, *77*, 3865-3868.

4. McKenna, K. P.; Hofer, F.; Gilks, D.; Lazarov, V. K.; Chen, C.; Wang Z.; Ikuhara, Y. *Nature Comm.* **2014**, *5*, 5740.

5. Heyd, J.; Scuseria, G. E.; Ernzerhof, M. *J. Chem. Phys.* **2003**, *118*, 8207-8215.